IEEE Photonics Journal
An IEEE Photonics Society Publication

Simultaneous Mid-Infrared Gas Sensing and Upconversion Based on Third Harmonic Generation in Cascaded Waveguides

Volume 12, Number 2, April 2020

Jianxing Pan
Zhenxing Chen
Tianye Huang
Shuwen Zeng
Zhuo Cheng
Pan Huang
Xiang Zhao
Perry Ping Shum
Gilberto Brambilla

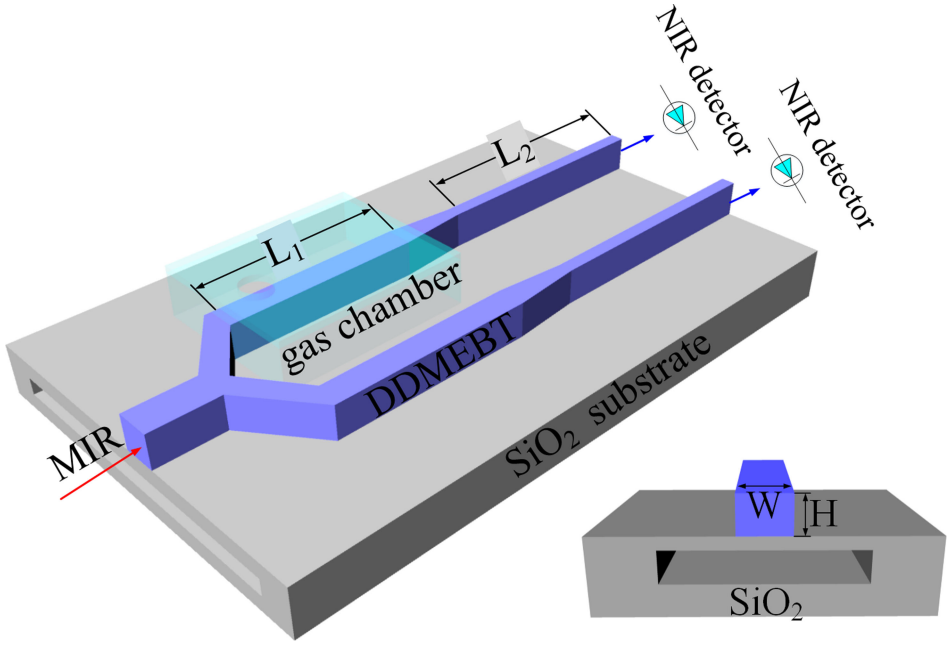

DOI: 10.1109/JPHOT.2020.2969975

Simultaneous Mid-Infrared Gas Sensing and Upconversion Based on Third Harmonic Generation in Cascaded Waveguides

Jianxing Pan,[1] Zhenxing Chen,[1] Tianye Huang,[1,2] Shuwen Zeng,[3] Zhuo Cheng,[1] Pan Huang,[1] Xiang Zhao,[1] Perry Ping Shum,[4] and Gilberto Brambilla[5]

[1]School of Mechanical Engineering and Electronic Information, China University of Geosciences (Wuhan), Wuhan 430074, China
[2]Wuhan National Laboratory for Optoelectronics, Wuhan 430074, China
[3]XLIM Research Institute, UMR 7252 CNRS/University of Limoges, Limoges 87060, France
[4]School of Electrical and Electronic Engineering, Center of Fiber Technology, Nanyang Technological University, Singapore 637553, Singapore
[5]Optoelectronics Research Centre, The University of Southampton, University Road, Southampton, SO17 1BJ, U.K.

DOI:10.1109/JPHOT.2020.2969975

Manuscript received October 6, 2019; revised January 17, 2020; accepted January 23, 2020. Date of publication January 27, 2020; date of current version March 9, 2020. This work was supported in part by Wuhan Science and Technology Bureau under Grant 2018010401011297, in part by the Open Project Program of Wuhan National Laboratory for Optoelectronics under Grant 2019WNLOKF005, in part by the Natural Science Foundation of Hubei Province under Grant 2019CFB598, in part by the National Natural Science Foundation of China under Grant 61605179, and in part by the Fundamental Research Funds for the Central Universities, China University of Geosciences (Wuhan) under Grants ZL201917, G1320311998, and 1910491B06. Corresponding author: Tianye Huang (e-mail: huangty@cug.edu.cn).

Abstract: The performance of conventional gas sensors based on light absorption in the mid-infrared are limited by the high-cost and low efficiency of photon detection at these wavelengths. In this paper, cascaded suspended waveguides are proposed and analyzed for mid-infrared gas sensing with enhanced detection limit. The cascaded structure contains two sections in which the first part is optimized for light absorption and the other one is tailored to satisfy the phase matching condition for third harmonic generation toward near-infrared wavelengths. In this configuration, the input mid-infrared light firstly experiences "fingerprint" frequency absorption in the on-chip gas chamber. Consequently, the residuary light produces third harmonic radiation in the second section. Benefiting from the nonlinear relation between pump and harmonic power, the sensitivity of the sensor is significantly improved. Moreover, the signal is up converted from mid-infrared to near-infrared and thus it can be easily detected by efficient near-infrared detectors. The results show that the detection limit can reach the order of nmol/L and the absorption lengths can be reduced to three times shorter comparing to direct mid-infrared detection. The proposed configuration has great potential for high performance on-chip gas sensing.

Index Terms: Photonic sensor, cascaded devices, suspended waveguides, third harmonic generation.

1. Introduction

Detecting the concentration of chemical vapor mixtures is of great demand in many fields such as environmental monitoring [1], resource prospecting [2], and medical diagnoses [3]. Analyzing the absorption at the "fingerprint" frequency is one of the most effective approaches for gas sensing. Conventional gas sensors based on this principle usually rely on free-space configuration with discrete components, which exhibit disadvantages such as bulky size and poor temporal stability. On-chip sensors, which benefit from the development of modern nano-fabrication technologies, can overcome these issues with a small footprint [4]. Current absorption gas sensors usually operate in the near-infrared (NIR), where photon detection can be performed with high efficiency and resolution ($\sim$fW). However, most of the fundamental vibrational and rotational modes of gas molecules are located in the mid-infrared (MIR) [5] where the absorption is much stronger (more than 100 times) compared to their NIR overtones. At ultra-low concentrations of methane, detection limit (DL) of $\sim 8.25 \times 10^{-8}$ mol/L has been reached using a ridge waveguide [6] while DL$\sim 1.1 \times 10^{-3}$ mol/L using a spiral waveguide [7]. However, gas sensing in the MIR also suffers from several challenges. For instance, MIR detectors are severely affected by thermal noise [8] and offer smaller and less uniform sensitive areas than their NIR counterparts [9]–[11]. In order to overcome these constrains, it is desirable that absorption occurs in the MIR while detection is performed in the NIR. Recently, nonlinear parametric upconversion methods demonstrated great potential for ultra-low noise single-photon imaging [12]. Leveraging on parametric processes, the information carried by MIR light is efficiently converted to NIR to achieve high performance photon detection. This upconversion-detection method has already been adopted for MIR gas sensing [11]. However, it should be noted that most of the previous upconversion-detection schemes are still limited in free-space implementations which are in bulk scales and not suitable for large-scale on-chip integration.

Third harmonic generation (THG), which converts three photons with lower frequency to a single photon with high frequency, is a promising approach to realize frequency upconversion over a large wavelength interval. Moreover, in the THG process, the generated harmonic power demonstrates a nearly third-order exponential relation with the pump power, which is favorable for sensitivity and DL enhancement. In the past few years, on-chip THGs have been investigated on different platforms such as photonic crystal [13], surface plasmon [14], [15], germanium-on-silicon [16], silicon nitride [17] and aluminum nitride [18]. However, such waveguides cannot be applied for MIR gas sensing directly as most of them are designed for NIR to visible conversion. Although some plasmonic waveguides have been proposed for efficient MIR to NIR conversion [19], it is still challenging to excite unconventional mode profiles in such waveguides.

In this paper, a cascaded organic waveguide made up of 2-[4-(dimethylamino)phenyl]-3-{[4-(dimethylamino)phenyl] ethynyl}buta-1,3-diene-1,1,4,4tetracarbonit-rile (DDMEBT) [20] is proposed for MIR absorptive gas sensing. Light absorption and frequency upconversion occur within two waveguide sections with different dimensions, respectively. The first one is optimized to enhance the light-gas interaction for efficient absorption, while the second one is designed for satisfying THG phase matching condition (PMC) between the fundamental mode in the MIR where the absorption peak of methane locates and the higher-order mode (HOM) in the NIR. By further employing the dual-branch structure, sensing performances are analyzed in detail. Results indicate that the proposed scheme is of great potential for on-chip gas sensing performance enhancement.

2. Methods

2.1 Principle and Theoretical Model

The schematic structure of the proposed sensor is shown in Fig. 1. In order to avoid the large absorption induced by the silicon dioxide (SiO_2) in the MIR, the substrate is partially etched as shown in the inset. The waveguide is formed by the organic material DDMEBT with highly nonlinear refractive index. The gas sensor is formed by two branches with the same structure in which one is used for gas sensing and the other is used as a reference. In particular, each branch contains

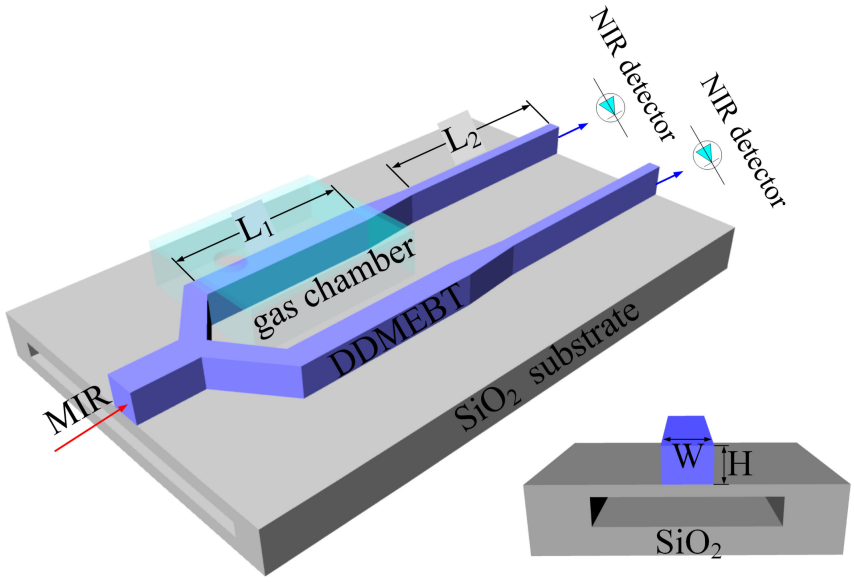

Fig. 1. Three-dimensional view of the cascaded DDMEBT waveguide structure.

two waveguides connected by a taper region. The input MIR light is split equally and injected into the two branches: in upper branch, light firstly interacts with gas in the on-chip chamber [7] and then converts to NIR through THG. While in lower branch, light does not interact with gas and thus experiences only intrinsic attenuation.

According to the Lambert-Beer's law, the relation between input and output powers at the gas chamber can be expressed by [6]:

$$P_{1,\mathrm{up}} = P_0 \exp(-\eta \varepsilon C L_1 - \alpha_{\mathrm{prop}} L_1) \tag{1}$$

where P_0 is the input power of the upper branch, ε is the molar absorption, C is the gas concentration, L_1 is the length of the first section of the waveguide, α_{prop} is the intrinsic absorption loss of the waveguide, and η is the confinement factor defined as [21]

$$\eta = \frac{\iint_{\mathrm{gas}} S_z dxdy}{\iint_{\mathrm{total}} S_z dxdy} \tag{2}$$

where S_z is the z component of the Poynting vector normal to the waveguide cross section. In the reference branch, due to the absence of the gas, the output power of the first section can be expressed by

$$P_{1,\mathrm{down}} = P_0 \exp(-\alpha_{\mathrm{prop}} L_1) \tag{3}$$

For the THG process in the second section of the waveguides, full-vectorial nonlinear coupled mode theory (CMT) is adopted. The equations describing the power transfer among the pump and the third harmonic waves can be written as [16]:

$$\frac{\partial E_1}{\partial z} = -\frac{1}{2}\alpha_1 \cdot E_1 + j\left(\gamma_1 |E_1|^2 + 2\gamma_{13}|E_3|^2\right) E_1 + j\gamma E_3 E_1^* E_1^* e^{j\Delta kz} \tag{4}$$

$$\frac{\partial E_3}{\partial z} = -\frac{1}{2}\alpha_3 \cdot E_3 + j\left(\gamma_3 |E_3|^2 + 2\gamma_{31}|E_1|^2\right) E_3 + j\gamma^* E_1 E_1 E_1 e^{-j\Delta kz} \tag{5}$$

where E_1 and E_3 represent the slowly varying field amplitudes for the pump and TH waves. The coefficients α_{i} ($i = 1, 3$) represent the loss. The term $\Delta k = k_{\mathrm{TH}} - 3k_{\mathrm{p}}$ is the phase mismatch between the pump and TH, with k_{TH} and k_{p} representing the propagation constants of TH and pump. Moreover, the nonlinear coefficients γ take into account the self-phase modulation (SPM),

cross-phase modulation (XPM) as well as THG effects, and are expressed as γ_1, γ_3, γ_{13}, γ_{31}, γ, $\gamma*$, respectively. For the theoretical analysis, under non-depletion approximation, the coupled-mode equations provide [22]:

$$P_3 \approx P_1^3 \gamma^2 \left(\frac{2}{\delta \tilde{k}}\right)^2 \sin^2\left(\frac{\delta k}{2} L_2\right) \tag{6}$$

where P_3 is the signal power after passing through the second waveguides, $\delta\tilde{k} = \delta k + (2\gamma_{31} - 3\gamma_1)P_0$ is the overall propagation mismatch, and L_2 is the length of the second waveguide. Considering a short propagation length, the approximate solution can be further simplified as:

$$P_3 \approx P_1^3 \gamma^2 L_2^2 \tag{7}$$

Substituting Eq. (7) into Eq. (1) and (3), we obtain

$$P_{3,\text{up}} \approx \left[P_0 \exp(-\eta\varepsilon C L_1 - \alpha_{\text{prop}} L_1)\right]^3 \gamma^2 L_2^2 \tag{8}$$

$$P_{3,\text{down}} \approx \left[P_0 \exp(-\alpha_{\text{prop}} L_1)\right]^3 \gamma^2 L_2^2 \tag{9}$$

The sensitivity is defined as the output power ratio variation between sensing and reference branches differential to the gas concentration

$$S_{\text{NIR}} = -\frac{\partial\left(P_{3,\text{up}}/P_{3,\text{down}}\right)}{\partial C} = 3\eta\varepsilon L_1 \exp(-3\eta\varepsilon C L_1) \tag{10}$$

If the detection is performed in MIR, the second waveguides are neglected and the corresponding sensitivity can be described as

$$S_{\text{MIR}} = -\frac{\partial\left(P_{1,\text{up}}/P_{1,\text{down}}\right)}{\partial C} = \eta\varepsilon L_1 \exp(-\eta\varepsilon C L_1) \tag{11}$$

Comparing Eq. (10) and Eq. (11), considering ultra-low gas concentration, the sensitivity obtained by NIR detection is roughly three times that of the one obtained by direct MIR detection. Furthermore, the optimal absorption length for NIR and MIR detection can be obtained as

$$L_{1opt\text{NIR}} = \frac{1}{3\eta\varepsilon C} \tag{12}$$

$$L_{1opt\text{MIR}} = \frac{1}{\eta\varepsilon C} \tag{13}$$

Obviously the optimal absorption waveguide length for MIR detection is roughly three times that of the NIR counterpart. For low concentration gas sensing, the DL is an important parameter to evaluate the sensing performance. Considering the smallest detectable power variation $P_{\min} = (P_{3,\text{down}} - P_{3,\text{up}})/\, P_{3,\text{down}}$ for NIR detector, the DL of the proposed scheme can be described as:

$$C_{\min} = \frac{-\ln\left(1 - \frac{RE}{P_0^3 \exp(-3\alpha_{\text{prop}} L_1)\gamma^2 L_2^2}\right)}{3\eta\varepsilon L_1} \tag{14}$$

where *RE* is the resolution of the NIR detector. In this paper, we set the *RE* of the NIR detector to be femtowatt according to Table 1, which can be achieved by the commercially-available components [23].

Since the sensor is based on intensity detection and the thermal-induced refractive index fluctuation can be mitigated by using mature thermal control, the intensity noise could be the main limitation. Intensity noise is the fluctuation in average power over a certain measurement time span and the intensity noise power after the first absorption waveguide can be described as [24]:

$$P_{RIN1} = \pm P_0 \sqrt{RIN \cdot B_e} \exp\left(-\eta\varepsilon C L_1 - \alpha_{\text{prop}} L_1\right) \tag{15}$$

where *RIN* is the relative intensity noise of the laser, B_e is the electrical bandwidth. Based on the Eq. (8), the intensity noise power after the second conversion waveguide can be approximately

TABLE 1
Comparison of Photodetectors at NIR and MIR

Material	Type	Wavelength range	Noise-equivalent power (NEP)	Cooler
HgCdTe	PDA10JT	2.0-5.4 μm (MIR)	1.84×10^{-10} W/Hz$^{1/2}$	yes
InGaAs	PDF10C	0.8-1.7 μm (NIR)	7.5×10^{-3} pW/Hz$^{1/2}$	no

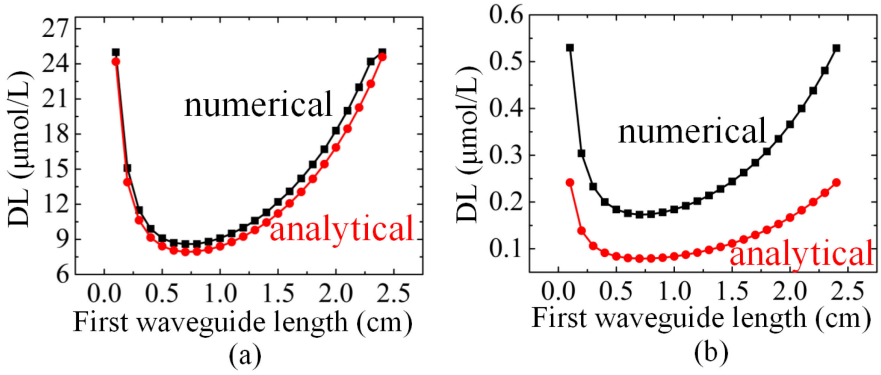

Fig. 2. Dependence of the DL on the first waveguide length at (a) 0.1 cm and (b) 1 cm length of the second waveguide. Numerical represents the exact solution, while analytical represents the approximate solution of eq. 14.

written as:

$$P_{RIN3} \approx \pm\left[P_0\sqrt{RIN \cdot B_e}\exp\left(-\eta\varepsilon CL_1 - \alpha_{\text{prop}}L_1\right)\right]^3\gamma^2L_2^2 \tag{16}$$

To satisfy the ultra-low concentration detecting, the *RIN* of the laser should be lower than the NEP of the detectors. Assuming that the methane concentration, input power and electrical bandwidth are 1 nmol/L, 50 mW and 10 MHz, respectively, the *RIN* of the laser should be less than −105 dBc/Hz when choosing the NIR detectors listed in Table 1. Such RIN requirement can be easily satisfied with commercially-available laser source [24].

Note that Eq. (14) is only an approximate solution of the DL, as it uses the approximate solution for the THG. To get the exact DL value, numerical calculation must be used. Firstly, the light-gas interaction in the first waveguide causes a variation in the pump power for THG in the second waveguide and then the NIR detector will detect a variation in the output. By assuming the variation of the output power caused by gas detection equal to the NIR detector resolution, the DL can be obtained by solving Eq. (4) and (5) to match such variation. For example, the numerical and analytical solutions of the DL with respect to the first waveguide length are investigated shown in Fig. 2. The numerical and analytical solutions are close at 0.1 cm but diverge at 1 cm length along the second THG waveguide.

2.2 Sensor Design

THG has been observed and measured in DDMEBT with determining a high THG susceptibility of $\chi^{(3)}_{1111} = 1.0 \pm 0.3 \times 10^{-19} m^2V^{-2}$ [20]. Besides, a metal-clad plasmonic double-slot waveguide with DDMEBT integrated into the slot region as the nonlinear material is proposed for THG up-conversion from the MIR to the NIR wavelength regime [25]. In our design, we choose this highly nonlinear material as the waveguide. As mentioned above, the light-gas interaction induced absorption occurs in the first waveguide, therefore it is important to ensure large evanescent fields in this section. In this paper, we consider methane sensing which possesses a “fingerprint” vibration

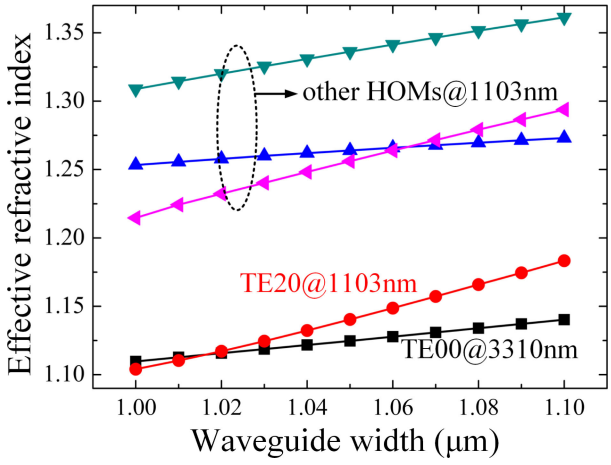

Fig. 3. Dependence of the effective refractive index of the TE_{20} mode, TE_{00} mode and other HOMs on waveguide width.

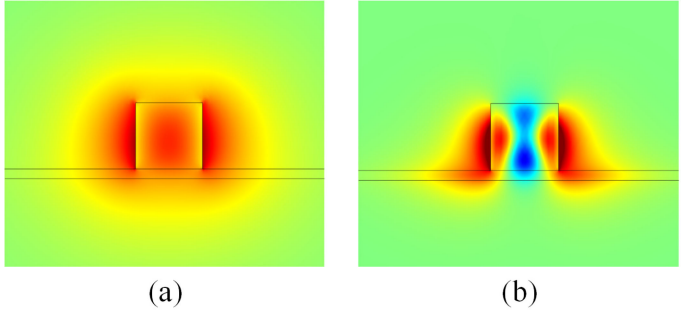

Fig. 4. Optical spatial distribution of (a) the fundamental TE_{00} mode and (b) the HOM TE_{20} mode.

near $\lambda\sim$3310 nm [7]. Furthermore, THG conversion should be avoided in this section, thus the phase mismatch has to be sufficient large between the injected MIR fundamental mode and any NIR higher-order mode (HOMs). For this purpose, by using a finite element method software, COMSOL, Fig. 3 plots the effective index of the fundamental mode at $\lambda\sim$3310 nm and HOMs at its harmonic wavelength when the waveguide height is 1010 nm. The DDMEBT refractive indices at $\lambda\sim$3310 nm and $\lambda\sim$1103.3 nm are 1.7690 and 1.8437, respectively.

When the waveguide width is around 1100 nm, the phase mismatch between fundamental mode and other HOMs is sufficient high, which means the upconversion is avoided in the first waveguide section. Meanwhile, the confinement factor reaches 53% indicating a large overlap with the target gas, which is essential for gas sensing. Based on the above analysis, the width and height of the first waveguide are determined to be 1100 nm and 1010 nm, respectively.

Different from the first waveguide section, the second one is mainly used for frequency upconversion, therefore it is important to fulfill the PMC and ensure sufficient mode overlap between the pump and harmonic modes. In Fig. 3, it is shown that PMC is satisfied between the pump TE_{00} mode and the harmonic TE_{20} HOM with waveguide width of 1016 nm. The corresponding effective indices for the modes are both 1.114. The mode profiles of these two modes are shown in Fig. 4. Although the TE_{20} mode has anti-phase side lobs, this portion is mainly distributed outside the waveguide where the nonlinear refractive index is negligible. Therefore, it will not induce significant negative impact on the THG nonlinearity [26]. In fact, according to our calculations, this mode offers the largest mode overlap for THG comparing to other HOMs with a nonlinear coupling coefficient γ as high as $\sim$0.28 $m^{-1}W^{-1}$.

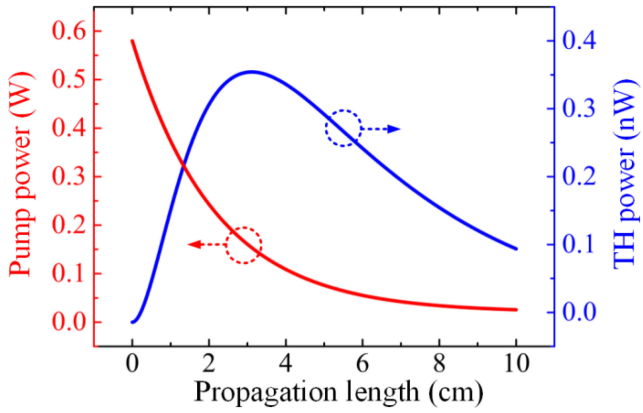

Fig. 5. Power of the TE_{00} and TE_{20} modes with respect to propagation distance.

TABLE 2
Parameters for Analyzing Sensing Performance

ε ($Lmol^{-1}cm^{-1}$)	γ_1 ($m^{-1}W^{-1}$)	γ_3 ($m^{-1}W^{-1}$)	γ ($m^{-1}W^{-1}$)	γ_{13} ($m^{-1}W^{-1}$)	γ_{31} ($m^{-1}W^{-1}$)	γ^* ($m^{-1}W^{-1}$)	η
382.5	0.82	8.43	0.28	1.03	3.09	0.28	53%

To analyze the THG performance of the second waveguide, we assume that a pump power of 50 mW. The losses at the pump and harmonic are 1 dB/cm and 0.5 dB/cm, respectively. By solving Eq. (4) and Eq. (5), the power evolution for both modes along the waveguide is shown in Fig. 5. At the beginning, the harmonic power raises because the gain provided by the pump overcomes the linear loss. However, with pump attenuation, the gain is no longer sufficient and the harmonic starts to decrease after reaching the conversion peak of 4.03 nW at 6.22 cm waveguide length.

3. Results

For gas sensing, the first waveguide section at upper branch is placed in the gas chamber filled with methane. Because of the interaction between evanescent field and gas, the pump experiences excess loss besides the intrinsic waveguide loss. After passing through the first section, the residual power is launched into the second one through a taper region to excite THG. The output variation ratio between the upper branch and the reference branch can then be employed to probe the gas concentration.

In this paper, we assume that the intrinsic losses of the first and second waveguides are equal and the intrinsic loss in the MIR is two times larger than that in the NIR. The relevant parameters for sensing performance evaluation are illustrated in Table 2.

To compare the sensing performances of the cascade sensing scheme and the MIR direct detection, the normalized power variations at different methane concentration are investigated shown in Fig. 6. The commercially-available photodetectors we choose for sensing performances comparison in the MIR and NIR wavelength regime are listed in Table 1. The noise-equivalent power (NEP) of NIR detector is 5 order of magnitude smaller than MIR detector. Additionally, the MIR detector needs thermoelectric cooler to hold the temperature at -30 °C which complicates the detection process. With an increased methane concentration, the normalized powers gradually decrease, but the cascaded sensing scheme demonstrates more pronounced variations than the direct detection. For cascaded sensing scheme, enhanced sensitivity can be obtained within the low concentration regime. At higher concentration, its sensitivity is still comparable with the direct detection.

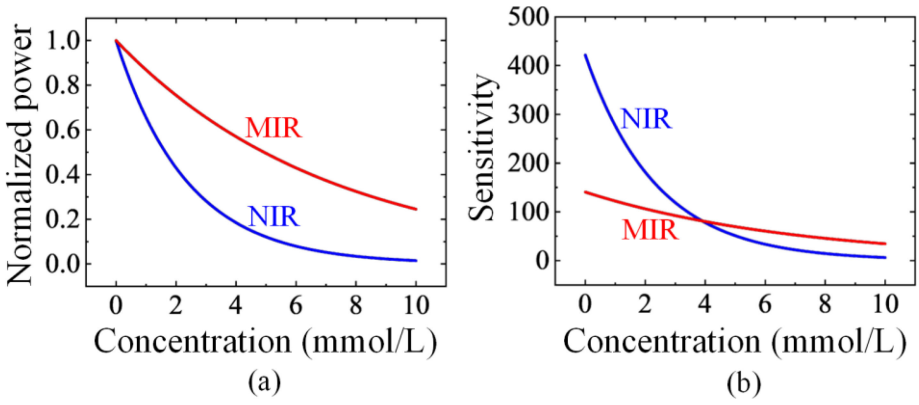

Fig. 6. (a) Normalized power and (b) sensitivity of the cascaded sensing scheme and the MIR direct detection with respect to different methane concentrations.

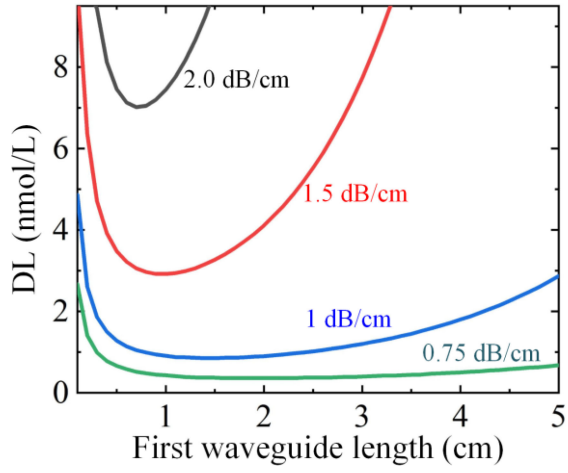

Fig. 7. Dependence of the DL on the first waveguide length L_1 for different MIR intrinsic losses.

In the following, the DL is analyzed by taking the sensor parameters such as intrinsic loss, input power, waveguide lengths and phase mismatch into account.

3.1 Intrinsic Loss

The waveguide intrinsic loss plays a significant role in the sensor sensitivity. If the waveguide loss is too high, it will dominate the absorption process and degrade the performance. Fig. 7 shows the DL with respect to the first waveguide length at different intrinsic MIR losses for a 50 mW pump power. According to the black curve denoting an intrinsic loss of 2 dB/cm, the DL initially decreases, reaching a minimum at the optimal length $L_{1\mathrm{opt}} = 0.7$ cm and then rises. When reducing the waveguide loss, the DL can be further enhanced with slightly longer interaction lengths. Furthermore, the DL becomes less sensitive to the waveguide length indicating a larger fabrication tolerance. In comparison, the direct MIR detection with intrinsic loss of 1 dB/cm [6] has an optimal absorption length of 4.3 cm which is three times longer. Therefore, the proposed scheme possesses the advantages of reducing the absorption length and this result is consistent with the above-mentioned theoretical analysis. As illustrated in Fig. 7, when the first waveguide is shorter than the optimal length, the DL is more sensitive to the length. This is due to the fact that most of the gas has yet been absorbed. On the contrary, when the first waveguide section is longer, the DL becomes less sensitive, but the variation slopes change significantly with loss. This can be

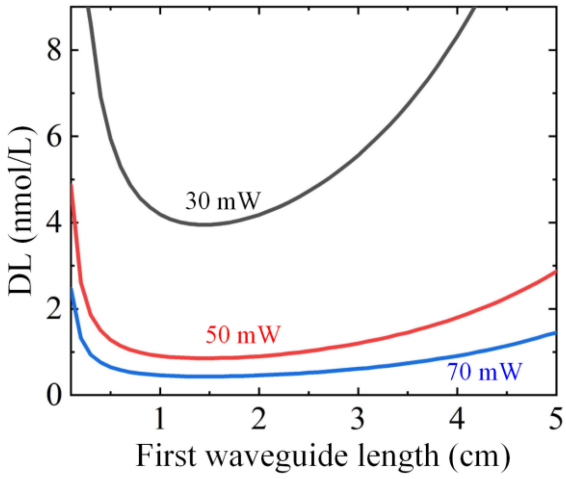

Fig. 8. Dependence of the DL with respect to the first waveguide length L_1 at different pump powers.

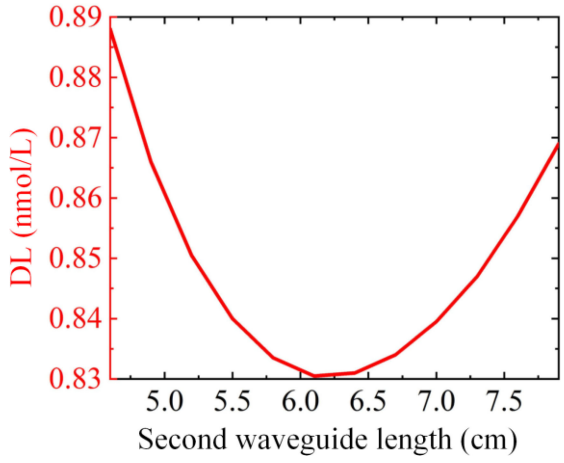

Fig. 9. Dependence of the DL on the second waveguide length L_2.

explained by the fact that excessively long absorption length with large intrinsic loss leads to lower pump powers for THG process.

3.2 Input Power

Fig. 8 shows the dependence of the DL on the input power P_0 with 1 dB/cm intrinsic loss [27]. With increasing pump powers, DL decreases. As shown in Fig. 8, the detection limit under optimal lengths of the waveguides can reach 3.95, 0.85, 0.43 nmol/L with 30 mW, 50 mW, 70 mW input power, respectively. The input power can be obtained from the commercially-available quantum cascade laser [6]. The optimal length of the first waveguide $L_{1\mathrm{opt}}$ changes little with the pump power. This is consistent with the former theoretical analysis. Furthermore, with the pump power increasing from 30 mW to 70 mW, the variations between the DLs at the optimal length $L_{1\mathrm{opt}}$ become smaller, indicating that there is a limit to enhance the DL by increasing the pump power.

3.3 Length of the Second Waveguide Section

To analyze the impacts of the second waveguide section L_2, the first waveguide length and MIR loss are fixed to the optimal length of 1.43 cm and 1 dB/cm, respectively. Fig. 9 shows the DL

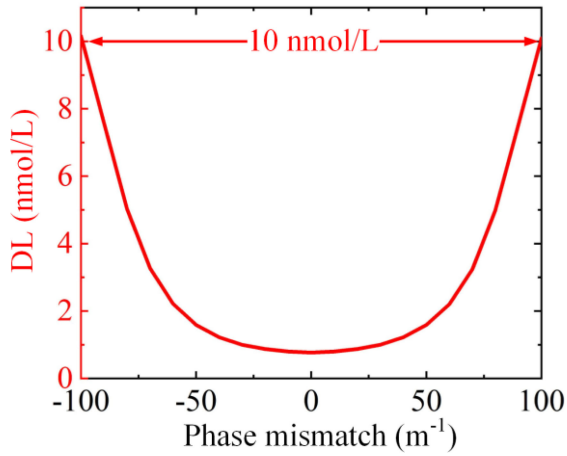

Fig. 10. Dependence of the DL on the phase mismatch Δk.

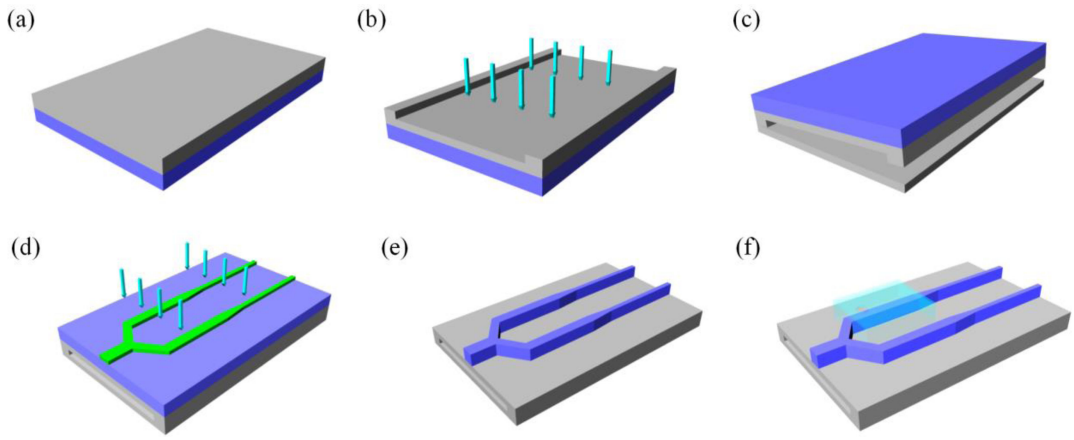

Fig. 11. A possible fabrication process flow: (a) deposition of DDMEBT on SiO_2 substrate and inversion, (b) formation of the suspended air trench, (c) SiO_2 hydrophobic bonding, (d) waveguide definition with metal mask and etching, (e) cascade waveguides for gas sensing and (f) on-chip gas chamber.

dependence on the second waveguide section L_2 with 50 mW input power. With L_2 increment, the DL first drops to a minimum and then rises showing a minimum of 0.43 nmol/L at the optimal length $L_{2\mathrm{opt}}$ of 6.22 cm. According to our calculation, such waveguide length corresponds to the location of peak THG efficiency. This is because a higher THG efficiency can enhance the power variation caused by the methane absorption and therefore lower methane concentrations can be detected.

3.4 Phase Mismatch

The phase mismatch δk is an important parameter for THG process since it determines the direction of power flow. Fig. 10 illustrates the dependence of DL on the phase mismatch. Considering a DL of 10 nmol/L, the phase mismatch tolerance is from -100 m^{-1} to 102 m^{-1}. Note that in the condition of high pump power, the phase mismatch tolerance will become less symmetric due to the nonlinear phase mismatch induced by the self-phase modulation and cross-phase modulation.

4. Conclusion

Figs. 11(a)–(f) show a possible fabrication process of the waveguide [28]. Firstly, the DDMEBT layer is grown on a SiO_2 substrate by heating the powder made of the organic material to 130

°C to generate a molecular beam directed onto the substrate (Fig. 11(a)). Traditional optical lithography with plasma reactive-ion etching is used to form the suspended trench (Fig. 11(b)). The etched die is then directly bonded onto the SiO_2 wafer by using the hydrophobic bonding techniques (Fig. 11(c)). Finally, a metal mask is used to define the ridge structure (Fig. 11(d)). The over-etching of the DDMEBT layer is accomplished by a plasma etching (Fig. 11(e)). Polydimethylsiloxane and the DDMEBT waveguide are thermally bonded to form an on-chip gas chamber.

In summary, an on-chip gas sensor with the capability of simultaneous MIR absorption and NIR upconversion detection is proposed. By tailoring the geometry parameters of the waveguides, PMC, large confinement factor and high nonlinear coefficient can be obtained simultaneously. The impacts of intrinsic loss, pump power, waveguide lengths, and phase mismatch on the DL are analyzed in detail. It is demonstrated that the proposed on-chip gas sensor can reduce the absorption length and improve the sensing performance with a DL as low as 0.43 nmol/L. The proposed scheme is of great potential for high performance on-chip gas sensing.

References

[1] P. A. Martin, "Near-infrared diode laser spectroscopy in chemical process and environmental air monitoring," *Chem. Soc. Rev.*, vol. 31, pp. 201–210, 2002.
[2] R. C. Schneider, and K. A. Kovar, "Analysis of ecstasy tablets: Comparison of reflectance and transmittance near infrared spectroscopy," *Forensic Sci. Int.*, vol. 134, pp. 187–195, 2003.
[3] S. Hocde *et al.*, "Metabolic imaging of tissues by infrared fiber-optic spectroscopy: An efficient tool for medical diagnosis," *J. Biomed. Opt.*, vol. 9, pp. 404–407, 2004.
[4] C. G. Li *et al.*, "A methane gas sensor based on mid-infrared quantum cascaded laser and multipass gas cell," *Spectrosc. Spec. Anal.*, vol. 36, pp. 1291–1295, 2016.
[5] J. Hodgkinson, and R. P. Tatam, "Optical gas sensing: A review," *Meas. Sci. Technol.*, vol. 24, 2013, Art. no. 012004.
[6] A. Gutierrez-Arroyo *et al.*, "Theoretical study of an evanescent optical integrated sensor for multipurpose detection of gases and liquids in the mid-infrared," *Sens. Actuators B.*, vol. 242, pp. 842–848, 2017.
[7] Z. Han *et al.*, "On-chip mid-infrared gas detection using Chalcogenide glass waveguide," *Appl. Phys. Lett.*, vol. 108, 2016, Art. no. 141106.
[8] S. Wolf *et al.*, "Self-gated mid-infrared short pulse upconversion detection for gas sensing," *Opt. Express*, vol. 25, pp. 24459–24468, 2017.
[9] S. D. Jackson, "Towards high-power mid-infrared emission from a fibre laser," *Nature Photon.*, vol. 6, pp. 423–431, 2012.
[10] T. W. Neely, T. A. Johnson, and S. A. Diddams, "High-power broadband laser source tunable from 3.0 μm to 4.4 μm based on a femtosecond Yb:Fiber oscillator," *Opt. Lett.*, vol. 36, pp. 4020–4022, 2011.
[11] L. Høgstedt *et al.*, "Low noise mid-ir upconversion detector for improved ir-degenerate four-wave mixing gas sensing," *Opt. Lett.*, vol. 39, pp. 5321–5324, 2014.
[12] J. S. Dam, P. Tidemand-Lichtenberg, and C. Pedersen, "Room-temperature mid-infrared single-photon spectral imaging," *Nature Photon.*, vol. 6, pp. 788–793, 2012.
[13] B. Corcoran *et al.*, "Green light emission in Silicon through slow-light enhanced third-harmonic generation in photonic-crystal waveguides," *Nature Photon.*, vol. 3, pp. 206–210, 2009.
[14] T. Huang *et al.*, "Internal asymmetric plasmonic slot waveguide for third harmonic generation with large fabrication tolerance," *Plasmonics*, vol. 16, pp. 1451–1459, 2016.
[15] T. Huang *et al.*, "Photon-Plasmon coupling for fundamental-mode phasematched third harmonic and triplet photon generation," *J. Lightw. Technol.*, vol. 36, no. 18, pp. 3892–3897, Sep. 2018.
[16] F. D. Leonardis, B. Troia, R. A. Soref, and V. M. N. Passaro, "Germanium-on-Silicon waveguide engineering for third harmonic generation in the mid-infrared," *J. Lightw. Technol.*, vol. 33, pp. 5103–5113, Dec. 2015.
[17] J. Pan, Z. Cheng, T. Huang, C. Song, P. P. Shum, and G. Brambilla, "Fundamental and third harmonic mode coupling induced single Soliton generation in kerr microresonators," *J. Lightw. Technol.*, vol. 37, no. 21, pp. 5531–5536, Nov. 2019.
[18] H. Jung, R. Stoll, X. Guo, D. Fischer, and H. X. Tang, "Green, red, and IR frequency comb line generation from single IR pump in AlN microring resonator," *Optica*, vol. 1, pp. 396–399. 2014.
[19] T. Huang *et al.*, "Efficient third-harmonic generation from 2 μm in asymmetric plasmonic slot waveguide," *IEEE Photon. J.*, vol. 6, no. 3, Jun. 2014, Art. no. 4800607.
[20] M. T. Beels *et al.*, "Compact TCBD based molecules and supramolecular assemblies for third-order nonlinear optics," *Opt. Mater. Express*, vol. 2, pp. 294–303, 2012.
[21] B. Kumari, A. Barh, R. K. Varshney, and B. P. Pal, "Silicon-on-nitride slot waveguide: A promising platform as mid-IR trace gas sensor," *Sens. Actuators B.*, vol. 236, pp. 759–764, 2016.
[22] A. Savchenko, "Glass micro-fibers for efficient third harmonic generation," *Opt. Express*, vol. 13, pp. 6798–6806, 2005.

[23] [Online]. Available: https://www.thorlabs.com
[24] Y. Huang, S. K. Kalyoncu, Q. Zhao, R. Torun, and O. Boyraz, "Silicon-on-Sapphire waveguides design for mid-IR evanescent field absorption gas sensors," *Opt. Commun.*, vol. 313, pp. 186–194, 2014.
[25] T. Wu *et al.*, "Efficient phase-matched third harmonic generation in a metal-clad plasmonic double-slot waveguide," *J. Opt.*, vol. 17, 2015, Art. no. 025506.
[26] T. Huang, P. M. Tagne and S. Fu, "Efficient second harmonic generation in internal asymmetric plasmonic slot waveguide," *Opt. Express.*, vol. 24, pp. 9706–9714, 2016.
[27] B. Esembeson, M. L. Scimeca, T. Michinobu, F. Diederich, and I. Biaggio, "A high-optical quality supramolecular assembly for third-order integrated nonlinear optics," *Adv. mater.*, vol. 20, pp. 4584–4587, 2008.
[28] J. Yuan *et al.*, "Mid-infrared octave-spanning supercontinuum and frequency comb generation in a suspended Germanium-membrane ridge waveguide," *J. Lightwave Technol.*, vol. 35, no. 14, pp. 2994–3002, Jul. 2015.